Millimeter-Wave MMIC Single-Pole-Double-Throw Passive HEMT Switches Using Impedance-Transformation Networks

Kun-You Lin, *Student Member, IEEE*, Yu-Jiu Wang, Dow-Chih Niu, and Huei Wang, *Senior Member, IEEE*

***Abstract*—This paper proposes a new design method for passive FET switches in the millimeter-wave (MMW) regime. In contrast to the conventional resonant-type switch design method, this passive FET switch circuit utilizes impedance transformation to compensate the drain–source capacitance effect for the off state at high frequencies. By means of this new design concept, a Q- and V-band monolithic-microwave integrated-circuit single-pole double-throw (SPDT) switches using a GaAs pseudomorphic high electron-mobility-transistor process are demonstrated. The Q-band SPDT switch has a measured isolation better than 30 dB for the off state and 2-dB insertion loss for the on state from 38 to 45 GHz, while the V-band switch also shows a measured isolation better than 30 dB for the off state and 4-dB insertion loss for the on state from 53 to 61 GHz. The obtained isolation performance using this design approach outmatches previously published FET switches in the MMW frequency range.**

***Index Terms*—High electron-mobility transistor (HEMT), millimeter wave (MMW), monolithic microwave integrated circuit (MMIC), switch.**

I. Introduction

SWITCHES ARE important components in microwave and millimeter-wave (MMW) systems. Monolithic p-i-n diode switches have demonstrated good performance even up to MMW frequency [1]. However, since the p-i-n diode process is not compatible with the high electron-mobility transistor (HEMT) monolithic-microwave integrated-circuit (MMIC) process, passive HEMT (or FET) switches are still very popular [2]–[12]. The reason is that they can be integrated with the other major building blocks in a MMW transmit/receive (T/R) module, which are mostly fabricated using the HEMT MMIC process. For frequencies of 20 GHz or lower, series and/or shunt configurations of a passive FET can readily serve as very good switches with excellent isolation and insertion-loss results demonstrated in [2] and [3]. However, at higher frequencies, the parasitic capacitance (mainly the drain-to-source capacitance $C_{\rm ds}$) will degrade the isolation performance significantly. Most MMW monolithic passive HEMT switches reported to date were parallel resonant-type FET switches [6], [7], with the isolation performance lower than 30 dB. A series resonant-type V-band SPDT passive HEMT switch demonstrated 3.9-dB insertion loss and 41-dB isolation at 59 GHz with a chip size of 3.3×1.7 mm^2 [8]. High-isolation Q-band HEMT switches reported in [9] utilized two-stage un-terminated quarter-wavelength shunt design to achieve up to 50-dB isolation. However, a huge chip area is required in such a design. The switching function at MMW range can also be achieved via a phase-cancellation technique using Lange couplers and demonstrated good isolation performance for a narrow bandwidth (28 dB at the Ka-band and 38 dB at the W-band) [10]. Since several 90° 3-dB hybrids were involved, the area requirement could still be a design drawback. Recently, compact dc–60-GHz heterojunction FET (HJFET) MMIC switches were reported with reasonable isolation performance [11], [12], but they required special process/layout for the ohmic electrode-sharing technology in the HEMT devices.

In this paper, a new HEMT switch design method using the impedance-transformation concept is proposed in contrast to the conventional resonant-type design for the MMW frequency. Q- and V-band single-pole double-throw (SPDT) MMIC switches using a standard 0.15-μm GaAs pseudomorphic high electron-mobility transistor (pHEMT) foundry process are designed, fabricated, and tested to verify this design concept. The Q-band switch demonstrated a measured on-state insertion loss of less than 2 dB with an off-state isolation of better than 30 dB from 38 to 45 GHz. The V-band switch demonstrated a measured on-state insertion loss of less than 4 dB with an off-state isolation of better than 30 dB from 53 to 61 GHz. The measured isolation results outmatch the reported Q- and V-band MMIC passive FET switches [4]–[6], [11]–[13] with slightly higher on-state insertion losses.

II. MMIC Process and Device Modeling

The HEMT device used in this design is the TRW standard 0.15-μm high-linearity InGaAs/AlGaAs/GaAs pHEMT MMIC process. The HEMT device has a typical unit current gain cutoff frequency (f_T) of 70 GHz and maximum oscillation frequency

Manuscript received May 29, 2002; revised November 3, 2002. This work was supported in part by the National Science Council under Research Project NSC 90-2219-E-002-007 and Research Project NSC 89-2213-E-002-178 and by the Minister of Education under the Research Excellence Program ME 89-E-FA06-2-4, R.O.C.

K.-Y. Lin and H. Wang are with the Department of Electrical Engineering and Graduate Institute of Communication Engineering, National Taiwan University, Taipei 106, Taiwan, R.O.C. (e-mail: hueiwang@ew.ee.ntu.edu.tw).

Y.-J. Wang was with the Department of Electrical Engineering, National Taiwan University, Taipei 106, Taiwan, R.O.C. He is now with the R.O.C. Navy.

D.-C. Niu is with the Chung-Shan Institute of Science and Technology (CSIST), Lung-Tang 325, Taiwan, R.O.C.

Digital Object Identifier 10.1109/TMTT.2003.809676

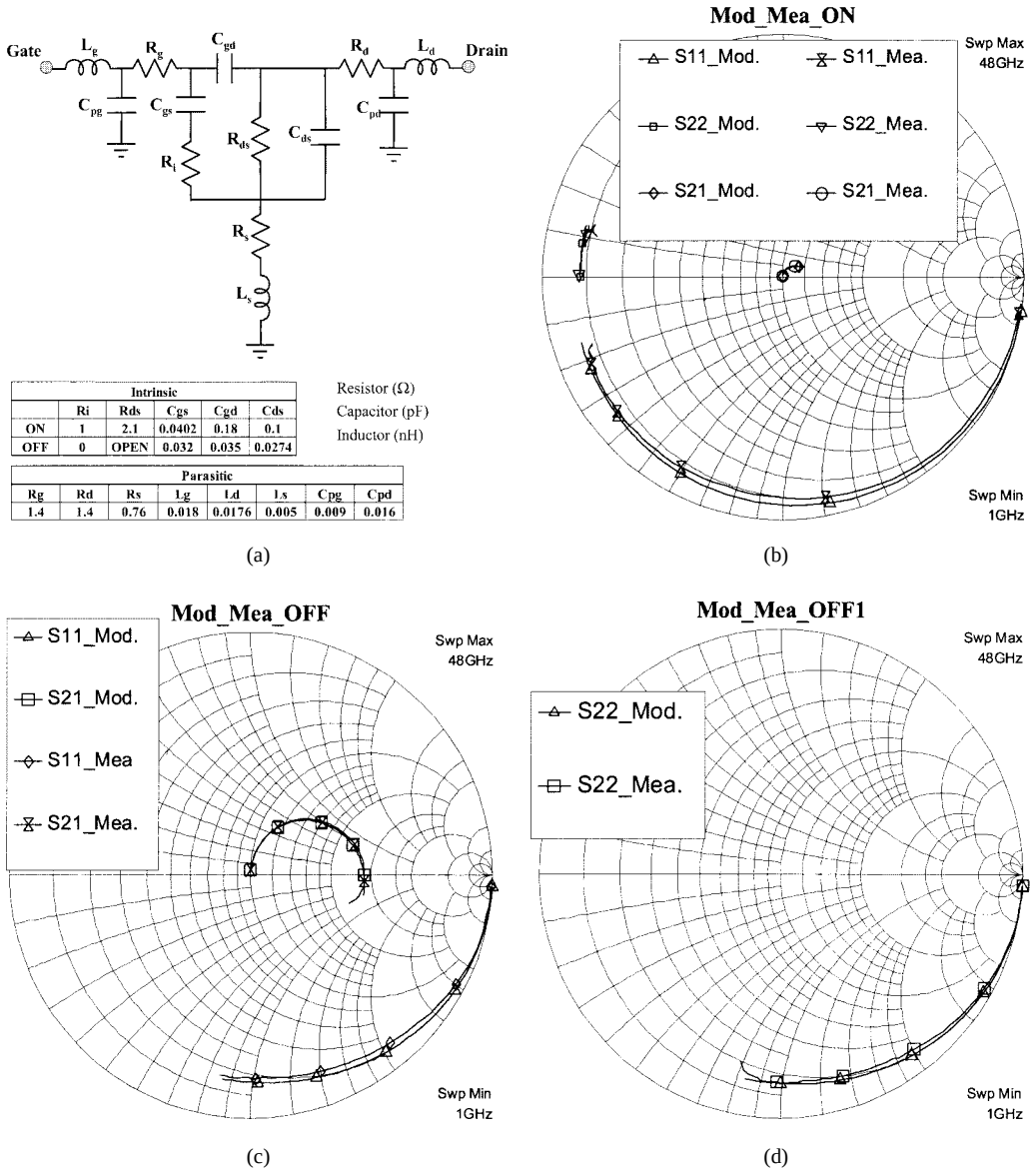

Fig. 1. (a) Small-signal equivalent circuit of the passive pHEMT model. The measured and simulated S-parameters of the: (b) on-state ($V_{\rm gs} = +0.3$ V) and (c) and (d) off-state ($V_{\rm gs} = -3$ V) passive HEMT.

($f_{\max}$) of 110 GHz, with a peak dc transconductance (G_m) of 580 mS/mm. The gate–drain breakdown voltage is 8 V, and the drain current at peak $G_m(I_{\rm dspk})$ at 5-V drain–source voltage is 280 mA/mm. Other passive components include thin-film resistors, metal–insulator–metal (MIM) capacitors, spiral inductors, and air bridges. The wafer is thinned to 4 mil for the gold plating of the backside and reactive ion etching via-holes are used for dc grounding.

The passive HEMT device model is developed by curve fitting the equivalent circuit to measured small-signal S-parameters of a common-source configuration to 48 GHz. Fig. 1(a) shows the small-signal equivalent-circuit models and the model parameters of the on state ($V_{\rm gs} = +0.3$ V) and off state ($V_{\rm gs} = -3$ V) of a four-finger 200-μm HEMT device. The modeled and measured on- and off-state small-signal S-parameters are shown in Fig. 1(b)–(d), respectively. The equivalent on-state series resistance of this passive HEMT is 2.1 Ω, while the off-state series capacitance is 27 fF.

III. Design Principle of Switches Using Impedance-Transformation Network

To design the impedance-transformation network for the passive HEMT switch, the input impedance of both on and off states need to be considered simultaneously. Let us use a design at 40 GHz with a 200-μm passive HEMT as an example. The matching network shown in Fig. 2 is composed with a series high impedance line, followed by an open stub and another series line. The input impedance values looking into points A–D for both on and off states (referred to schematic diagram of Fig. 2) were indicated on the Smith chart, shown in Fig. 3. As observed on the Smith chart, the input impedance values of both the on and off states for a nonresonant shunt FET (point A's) can be successfully transferred to a near by short circuit (small resistor) and a near by open circuit (point D's), respectively, through the same impedance-transformation network by carefully selecting the length of each high-impedance line.

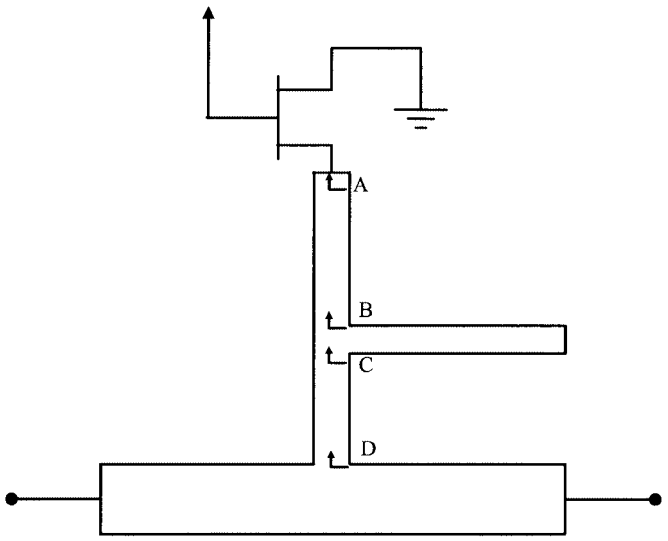

Fig. 2. Schematic of an FET in series with the impedance-transformation network.

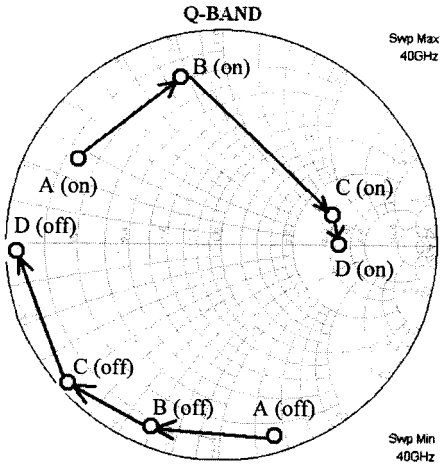

Fig. 3. Input impedances looking into points A–D of the passive switch with the impedance-transformation network in Fig. 2 on the Smith chart for both on and off states at 40 GHz.

IV. Comparison With Resonant-Type Switches

A passive FET switch can be realized by either a shunt or series configuration. Several passive HEMT SPDT shunt configurations were reported [6]–[9]. They were either directly shunt to ground [6], [7] or shunt with a quarter-wavelength line [9]. In order to compare the conventional resonant method and our proposed method in designing MMW switches using the shunt configuration, a four-finger 200-μm passive HEMT is studied in each case at 40 GHz. Fig. 4(a) shows the schematic diagram of a resonant-type SPST switch with a shunt configuration, and a high-impedance line is used to resonant out the off-state capacitor. The on- and off-state impedances of the shunt resonated HEMT are shown in Fig. 4(b). The off-state impedance of the resonant HEMT is very high (1310 Ω), but the on-state impedance is not too low $(3.33+j5.47\,\Omega)$ due to the parasitic inductance of the HEMT. The resonant-type shunt SPST switches have very good insertion-loss performance (0.163 dB) but its

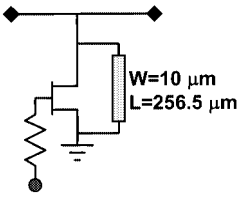

(a)

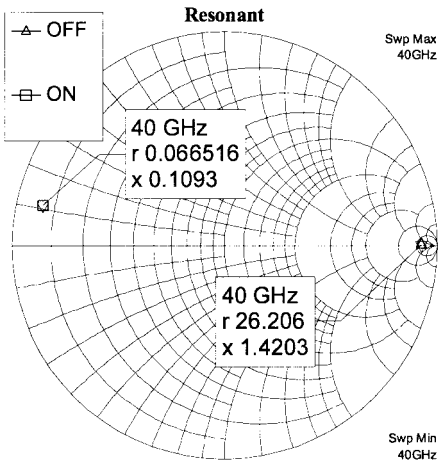

(b)

Fig. 4. (a) Schematic diagram of a resonant SPST switch using a shunt resonated HEMT. (b) On- and off-state impedances of a resonated HEMT shown in a Smith chart.

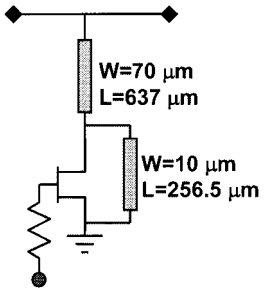

(a)

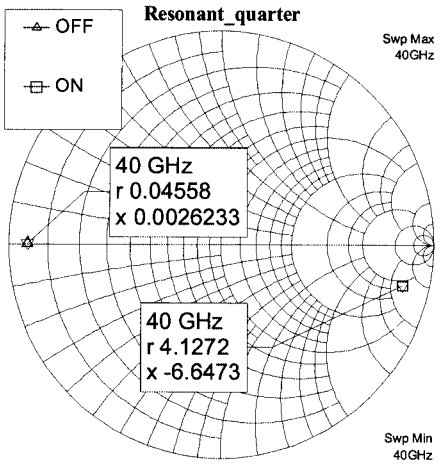

(b)

Fig. 5. (a) Schematic diagram of an SPST switch using a shunt resonated HEMT series with a quarter-wavelength 50-Ω transmission line. (b) On- and off-state impedances of a resonated HEMT series with a quarter-wavelength 50-Ω transmission line shown in a Smith chart.

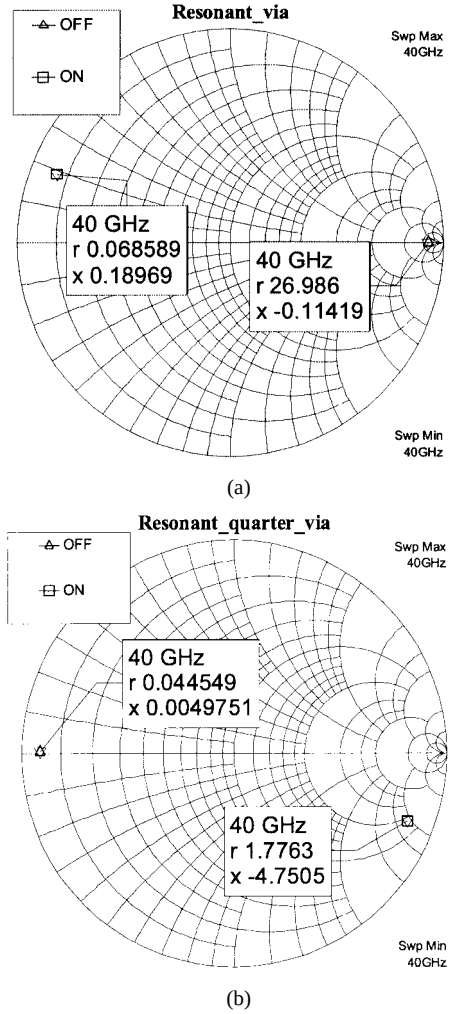

Fig. 6. On- and off-state impedances of (a) a shunt resonated HEMT and (b) resonated HEMT series with a quarter-wavelength 50-Ω transmission line including the via-hole effect on a Smith chart.

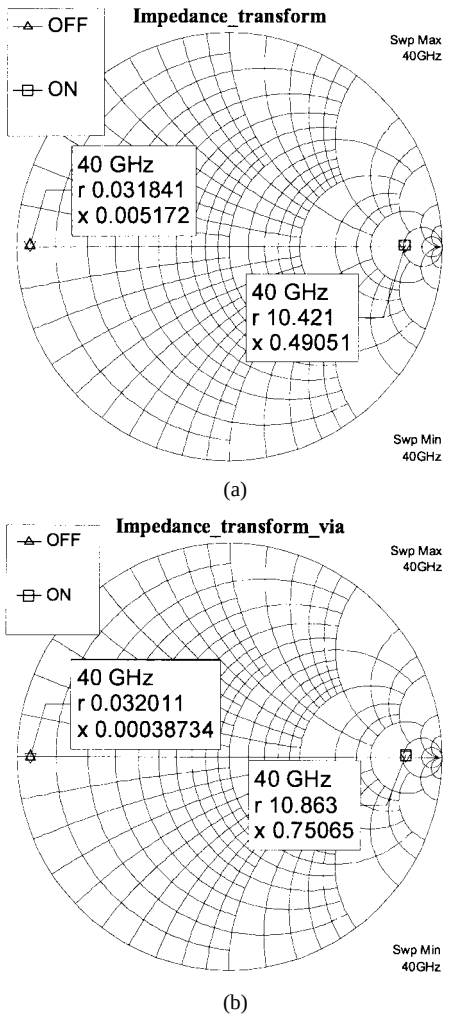

Fig. 7. On- and off-state impedances of a four-finger 200-μm passive HEMT using an impedance-transformation network: (a) without and (b) with the via-hole effect.

isolation is poor (13.08 dB). In order to improve the isolation of resonant-type shunt switches, we can add a quarter-wavelength 50-Ω transmission line to the shunt resonated HEMT (shown in Fig. 5). The off-state impedance is transformed to a low impedance (2.28 Ω), and the on-state impedance is transformed to a high impedance $(206 - j332\ \Omega)$. The isolation is improved to 21.55 dB, and the insertion loss degrades slightly to 0.3 dB.

In the MMW frequency range, the via-hole effect needs to be considered in the circuit design since the equivalent inductance is significant enough to affect the circuit performance. Fig. 6 shows the impedances of a shunt resonated HEMT and a shunt resonated HEMT series with a quarter-wavelength 50-Ω line including the via-hole effect ($\sim$15 pH, two via-holes in parallel). The isolation of a resonant-type shunt SPST switch from 13.08 dB becomes 9.46 dB when the via-hole is considered. By using the resonant approach, the via-hole effect makes the on-state impedance of a resonant HEMT increase with frequency and, thus, degrades the isolation performance of the switch.

On the other hand, Fig. 7 shows the on- and off-state impedances of a four-finger 200-μm passive HEMT using an impedance-transformation network without/with the via-hole effect. It can be observed that the performances of the SPST switches using an impedance-transformation network are not affected by the via-hole. The impedances and SPST switch performances of different approaches are summarized in Table I. The SPST switch using the resonant technique has poor isolation, but very good insertion loss.

V. SPDT Switches Using Impedance-Transformation Network

In our design, the inductor to resonate the passive HEMT is replaced by the impedance-transformation network series to the HEMT device, and then the HEMT with the transformation network is shunt to ground to serve the switching function. The schematic diagram of the design is presented in Fig. 2.

The device size selection of a passive FET switch design affects both the insertion loss and isolation performance. Usually, for a series passive FET with a small periphery, the series on-state resistance is high, while the off-state drain-to-source capacitance $(C_{\rm ds})$ is low, thus, it exhibits a tradeoff for a good isolation, high insertion loss, and low power-handling

TABLE I
IMPEDANCES AND SPST SWITCH RESULTS OF DIFFERENT TECHNIQUES

	On-state impedance (Ω)	Off-state impedance (Ω)	Insertion Loss (dB)	Isolation (dB)
HEMT	4 + j 5.78 (Γ=0.8537∠166.7°)	1.65 - j 60.534 (Γ=0.9736∠-79.09°)	0.766	12.48
Resonated HEMT	3.33 + j 5.47 (Γ=0.8767∠167.47°)	1310 (Γ=0.9267∠0°)	0.163	13.08
Resonated HEMT + λ/4	206 - j 332 (Γ=0.8751∠-12.45°)	2.28 (Γ=0.9128∠180°)	0.3	21.55
Resonated HEMT with via hole	3.43 + j 9.48 (Γ=0.8758∠158.42°)	1349 (Γ=0.9285∠0°)	0.16	9.46
Resonated HEMT with via hole + λ/4	88.82 - j 237.52 (Γ=0.87∠-21.02°)	2.23 (Γ=0.9147∠180°)	0.33	21.69
Impedance transformation	521 (Γ=0.8253∠0°)	1.592 (Γ=0.9383∠180°)	0.41	24.34
Impedance transformation with via hole	543 (Γ=0.8322∠0°)	1.6 (Γ=0.938∠180°)	0.39	24.41

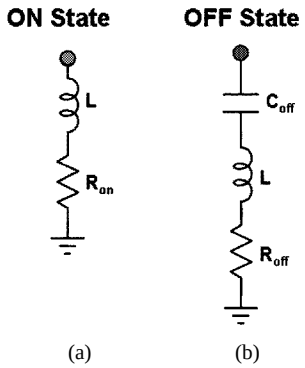

Fig. 8. Simplified models for: (a) on- and (b) off-state passive HEMTs.

capability. On the other hand, a large device conducts the opposite behavior, i.e., low insertion loss and poor isolation. In our design, since an impedance transformation is involved, this analysis is accompanied with the impedance-transformation network. In order to simply the analysis, the simplified model shown in Fig. 8 is used instead of the complete model shown in Fig. 1(a). The on-state model is represented as an inductor series with a resistor, and the off-state model is represented as an inductor series with a resistor and capacitor. Fig. 9 shows the simulated S-parameters from 1 to 50 GHz of the simplified models and the complete model S-parameters of a 120- and 200-μm HEMT. The agreement indicates the validity to use the simplified models. The model parameters related to the device gatewidth $W_g(\mu\text{m})$ are shown as follows:

$$\begin{aligned} L &= 0.115 \times 10^{-12} \times W_s(\text{H}) \\ R_{\text{on}} &= \frac{800}{W_g}\,(\Omega) \\ C_{\text{off}} &= 0.3 \times 10^{-15} \times W_g(\text{F}) \\ R_{\text{off}} &= \frac{330}{W_g}\,(\Omega). \end{aligned} \tag{1}$$

In the device size selection, the effect of the third transmission line can be neglected (Fig. 10) since it is found not to be very crucial. The on- and off-state input impedances looking into the transistor are

$$\begin{aligned} Z_{\text{on}} &= R_{\text{on}} + jX_{\text{on}} \\ R_{\text{on}} &= \frac{800}{W_g}\,(\Omega) \\ X_{\text{on}} &= \omega \times 0.115 \times \times 10^{-12} \times W_g \\ Z_{\text{off}} &= R_{\text{off}} + jX_{\text{off}} \\ R_{\text{off}} &= \frac{330}{W_g}\,(\Omega) \\ X_{\text{off}} &= \omega \times 0.115 \times 10^{-12} \times W_g - \frac{1}{\omega \times 0.3 \times 10^{-15} \times W_g}. \end{aligned} \tag{2}$$

After a series transmission line with characteristic impedance Z_1 and electric length θ_1, the input on- and off-state impedances are

$$Z_{i1,\text{on}} = Z_{01}\frac{R_{\text{on}} + j(X_{\text{on}} + Z_{01}\tan\theta_1)}{Z_{01} - X_{\text{on}}\tan\theta_1 + jR_{\text{on}}\tan\theta_1}$$

and

$$Z_{i1,\text{off}} = Z_{01}\frac{R_{\text{off}} + j(X_{\text{off}} + Z_{01}\tan\theta_1)}{Z_{01} - X_{\text{off}}\tan\theta_1 + jR_{\text{off}}\tan\theta_1}. \tag{3}$$

The imaginary part of $Z_{i,\text{off}}$ is zero, then we have

$$\begin{aligned} &\tan\theta_1 \\ &= \frac{-\left(X_{\text{off}}^2 + R_{\text{off}}^2 - Z_{01}^2\right) \pm \sqrt{\left(X_{\text{off}}^2 + R_{\text{off}}^2 - Z_{01}^2\right)^2 + 4Z_{01}^2X_{\text{off}}^2}}{2Z_{01}X_{\text{off}}}. \end{aligned} \tag{4}$$

Finally after the shunt open stub (Z_2, θ_2), the input impedance is

$$Z_{i2,\text{on}} = \frac{-jZ_{i1,\text{on}}Z_{02}}{Z_{i1,\text{on}}\tan\theta_2 - jZ_{02}}. \tag{5}$$

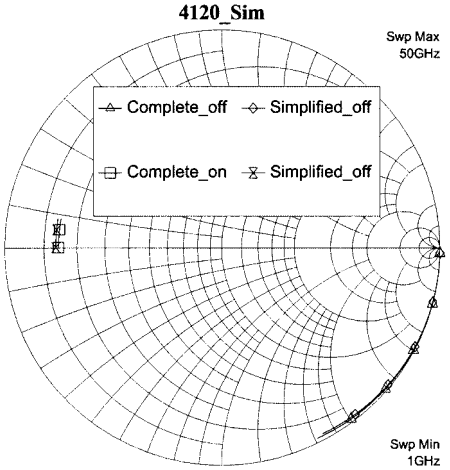

(a)

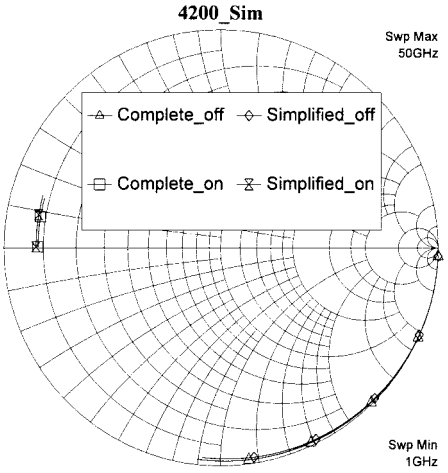

(b)

Fig. 9. On- and off-state S-parameters of a: (a) 120- and (b) 200-μm passive HEMT for the simplified and complete models.

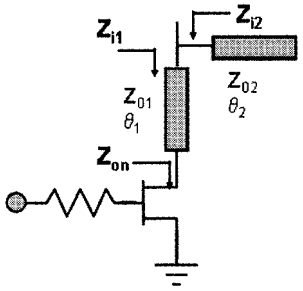

Fig. 10. Schematic of a passive HEMT with impedance-transformation network.

Since the impedance of the open stub is very high compared with $Z_{i1,\mathrm{off}}$, $Z_{i2,\mathrm{off}}$ is equal to $Z_{i1,\mathrm{off}}$. We let the imaginary of $Z_{i2,\mathrm{on}}$ be zero. We then get

$$\tan\theta_2 = -Z_{02}\mathrm{Im}\{Y_{i1,\mathrm{on}}\}. \tag{6}$$

For the given impedances of the transmission lines, $Z_{i2,\mathrm{on}}$ and $Z_{i2,\mathrm{off}}$ can be solved. Fig. 11 shows the on- and off-state impedances of a passive HEMT with an impedance-transformation network versus device gate periphery (W_g) at 40 GHz. The impedances of the series and shunt transmission lines are 90 and 60 Ω, respectively. The best on-state impedance and the worst off-state

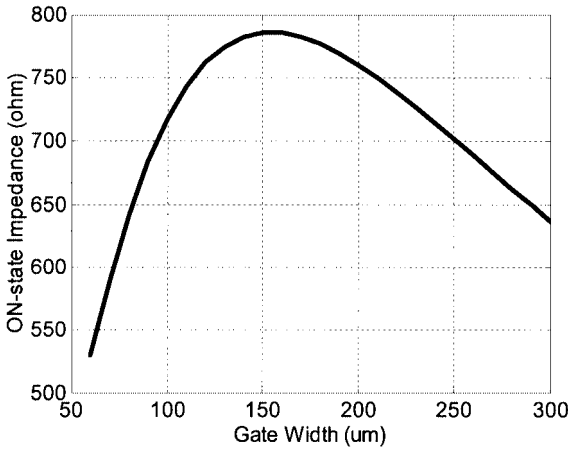

(a)

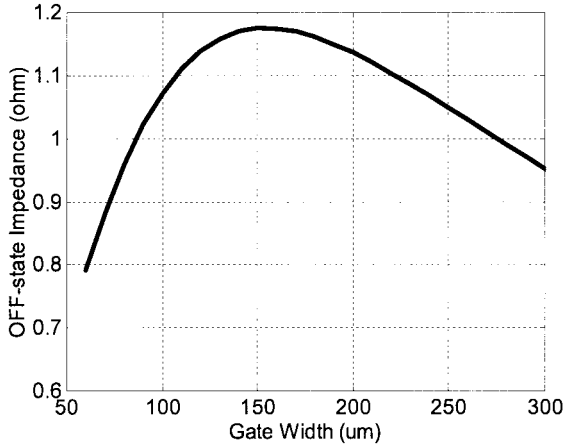

(b)

Fig. 11. (a) On- and (b) off-state impedances of shunt passive HEMTs with an impedance-transformation network versus device gate periphery at 40 GHz.

impedance occur at approximately a 160-μm gate periphery. We selected the device of a 200-μm HEMT for our design.

In order to avoid the uncertainty of the passive-element models in the MMW frequency and the coupling effects between elements, the entire matching structures have been analyzed using full-wave electromagnetic (EM) simulation [14] in the final circuit simulation. The complete SPDT switch circuit schematic diagram for both the Q- and V-band designs are shown in Fig. 12. In each path, two cascaded shunt passive HEMT devices with the impedance-transformation networks were used to enhance the isolation. The chip photographs are shown in Fig. 13(a) and (b), with a common chip size of 2 mm $\times$ 1 mm.

VI. Measurement Results

Both the Q- and V-band SPDT MMIC switches were measured via on-wafer probing. The on- and off-state two-port small-signal S-parameters of each path were obtained by terminating the output port of the other path. The control voltage for each path is $+0.5$ V for the on state and -3 V for the off state. For the Q-band design, the on-state insertion loss and off-state isolation from 30 to 50 GHz are plotted in Fig. 14(a) with insertion loss less than 2 dB and isolation better than 30 dB from 38 to 45 GHz. The best isolation is 43 dB around 41 GHz. Fig. 14(b) shows the V-band SPDT results

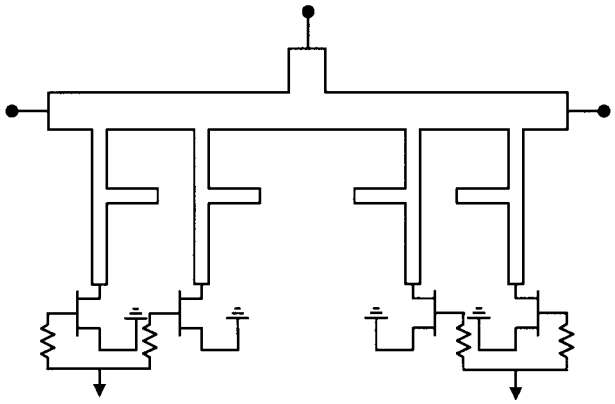

Fig. 12. Complete schematic diagram of the SPDT switch using shunt passive HEMTs with an impedance-transformation network.

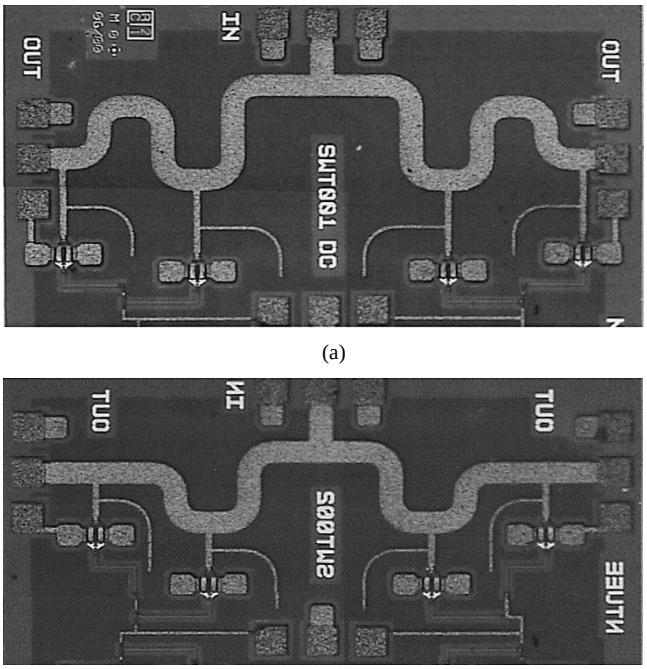

Fig. 13. Chip photographs of the: (a) Q- and (b) V-band MMIC SPDT switches with a common chip size of 2 mm × 1 mm.

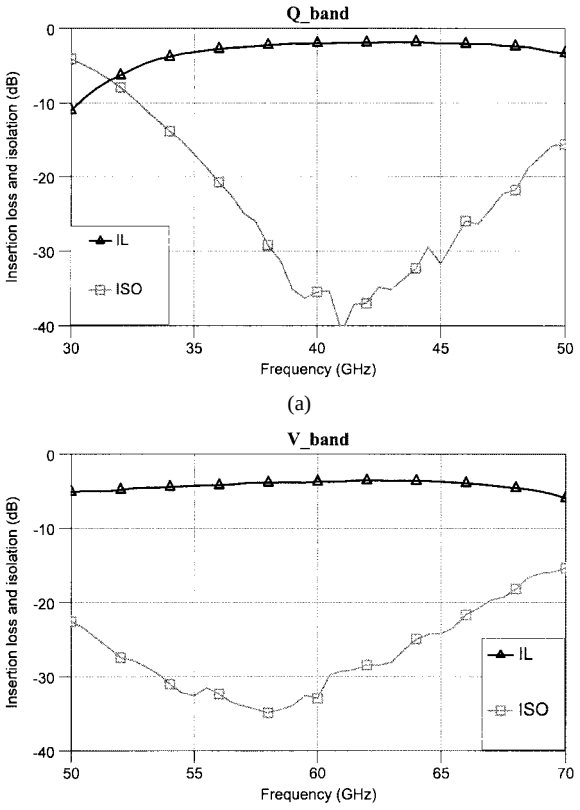

Fig. 14. Measured on-state insertion loss and off-state isolation of the: (a) Q- and (b) V-band switches.

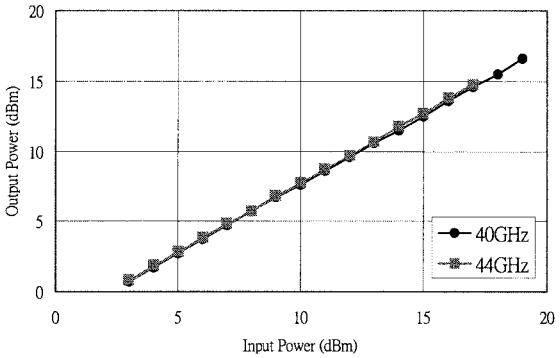

Fig. 15. Measured output power versus input power of the Q-band switch at 40 and 44 GHz.

from 50 to 70 GHz. The insertion loss is from 3.5 to 4 dB and the isolation is better than 30 dB from 53 to 61 GHz. The best isolation is 35 dB at approximately 58 GHz.

The output power $(P_{\rm out})$ versus input power $(P_{\rm in})$ measurement were also exercised at 40 and 44 GHz for the Q-band MMIC chip. Owing to the power limitation of input source, we could only measure up to 17-dBm input power for 44 GHz and 19 dBm for 40 GHz. The $P_{\rm out}$ versus $P_{\rm in}$ curves were plotted in Fig. 15. As indicated from the measured data, only 0.2-dB compression was observed at 40 GHz for $P_{\rm out}$ of 19 dBm. The third-order intercept point (IP3) test was also attempted. However, also due to a lack of a sufficient high power source and the limited dynamic range of the spectrum analyzer, we could not obtain accurate IP3 measurement results. A rough estimated output IP3 of the Q-band MMIC SPDT switch from the $P_{\rm out}$ versus $P_{\rm in}$ data should be much higher than 30 dBm. The output power compression performance (0.2 dB at 40 GHz for $P_{\rm out}$ of 19 dBm) is better than that reported in [11] (1-dB at 40 GHz for $P_{\rm out}$ of 20 dBm). Further considering for the device periphery, the compression performance of our design is still at least comparable to that in [11]. It is noted that the gate periphery of the HEMT device in ours is 200 μm, while that in [11] is 100 μm.

To verify our design and simulation methodology in the MMIC design, the simulated small-signal performance for the Q- and V-band switches were compared with the measured results. Fig. 16(a) shows the output return loss and isolation of the off state, while Fig. 16(b) and (c) presents the output return loss and insertion loss of the on state and input return losses from 30 to 50 GHz. Fig. 17(a) shows the output return loss and isolation of the off state, while Fig. 17(b) and (c) presents the output return loss and insertion loss of the on state and

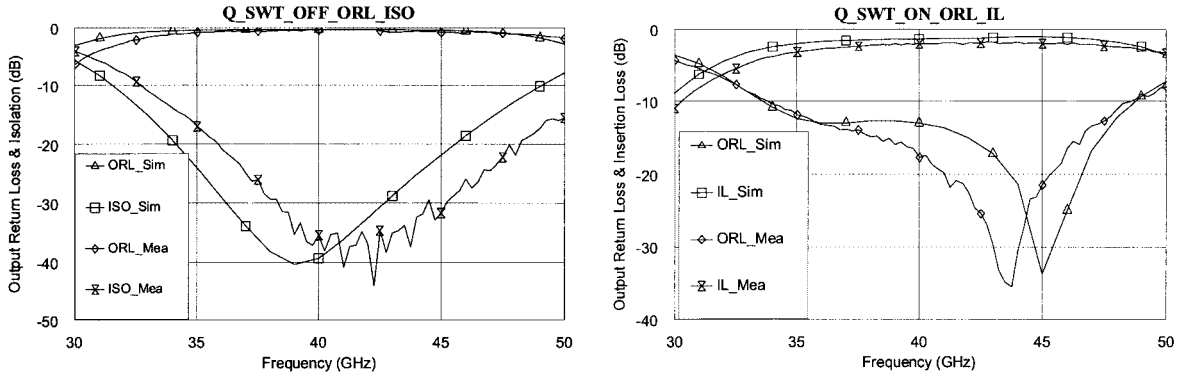

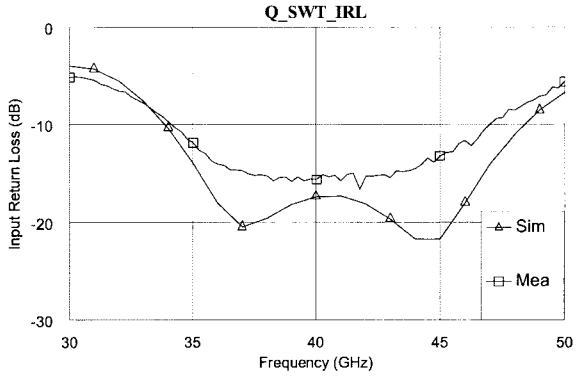

Fig. 16. Simulated and measured results of: (a) output return loss and isolation of the off state, (b) output return loss and insertion loss of the on state, and (c) input return loss from 30 to 50 GHz for the Q-band switch.

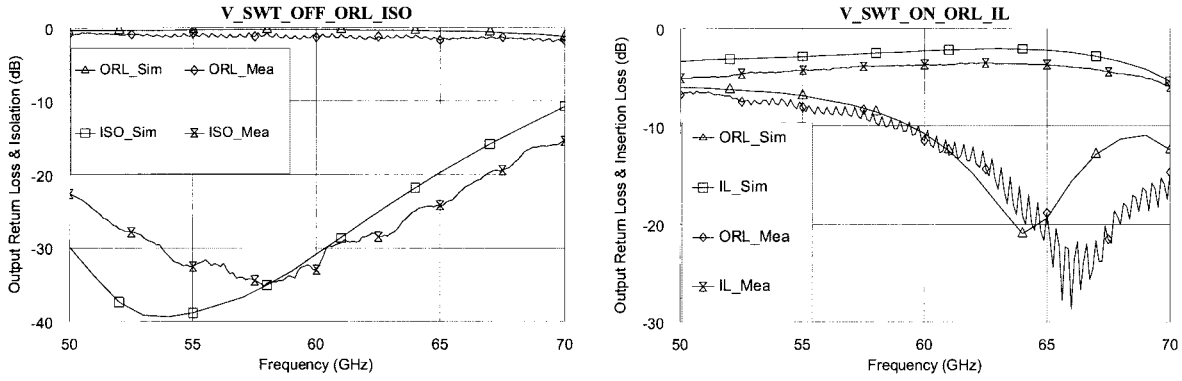

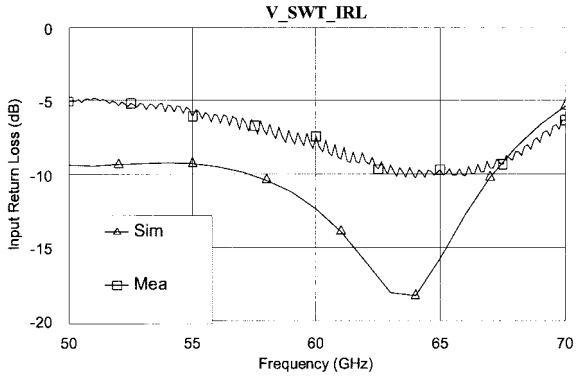

Fig. 17. Simulated and measured results of: (a) output return loss and isolation of the off state, (b) output return loss and insertion loss of the on state, and (c) input return loss from 50 to 70 GHz for the V-band switch.

TABLE II
SUMMARY OF THE PERFORMANCE AND FEATURES FOR PREVIOUSLY REPORTED PASSIVE HEMT MMIC SWITCHES AND THIS STUDY FROM Ka- TO W-BAND

Author	Device	Design Approach	Number of Stage	Freq. Range (GHz)	Insertion Loss (dB)	Isolation (dB)	Chip Size (mm^2)
Schindler et al. (Raytheon) [4]	MESFET	Shunt	2	20-40	2@40 GHz	25-28	—
Bernkopf et al. (Raytheon) [5]	MESFET	Shunt	2	15-30	2-3	> 20	2x2.2
Lan et al. (Hughes) [6]	MESFET	Shunt	2	56-64	< 3.2	> 23	0.8x2
Madihian et al. (NEC) [8]	HJFET	Series resonant, Shunt	2	57-61	3.9 (Min)	41 (Max)	3.3x1.7
Ingram et al. (TRW) [9]	GaAs HEMT	Quarter-wavelength, shunt	2	42-46	< 1.6	35-50	5x2
Mizutani et al. (NEC) [11]	HJFET	Series-shunt; Ohmic electrode-sharing technology (special process/layout required)	—	DC-40 (SPDT) DC-60 (SPST)	< 3.5 (SPDT)	> 25 (SPDT)	0.86x0.64
Lo et al. (TRW) [10]	InP HEMT	Phase cancellation using 90° Lange couplers	—	33-38	—	18-28	1.8x2.4*
Lo et al. (TRW) [10]	GaAs HEMT	Phase cancellation using 90° Lange couplers	—	92-95	—	28-38	1.3x2.2*
Hieda et al. (Mitsubishi) [13]	GaAs FET	Series-shunt	2	28	3.1	28.9	1.64x1.34
This work	GaAs HEMT	Shunt with impedance transformation network	2	38-43	< 2	> 30	2x1
This work	GaAs HEMT	Shunt with impedance transformation network	2	53-61	< 4	> 30	2x1

* Area of switch portion estimated from the entire MMIC chip (LNA + switch) [10].

input return losses from 50 to 70 GHz. The simulated results reasonably agree with the measured performance.

Table II summarizes the previously reported performance and features of passive FET MMIC switches from the Ka- to W-band. The isolation of the Q-band switches [9] achieved the best isolation at the cost of large chip area. Our Q-band switch shows better isolation than all the other reported results at similar frequencies [4], [5]. For V-band switches, the isolation performance in this study outmatches the other designs at similar frequencies [6], [11] with a comparable chip size of [6], and a slightly higher on-state insertion loss. Compare to [8], our design has better insertion loss, bandwidth, smaller chip size, and a slightly lower isolation. It is observed that the isolation results of the passive FET switches using impedance-transformation networks are better than those of other types of reported MMIC FET switches [4]–[6], [11]–[13].

VII. SUMMARY

We have demonstrated a new methodology for passive FET switch design using impedance transformation in the MMW frequency range. Q- and V-band SPDT MMIC switches using the GaAs pHEMT MMIC process were designed and fabricated to verify this design concept. The Q-band switch has a measured isolation better than 30 dB from 38 to 45 GHz, while the V-band switch also shows a measured isolation better than 30 dB from 53 to 61 GHz, which outmatch previously published FET switches in the MMW frequency range.

ACKNOWLEDGMENT

The MMIC foundry service was provided by TRW Inc., Redondo Beach, CA, through the Chip Implement Center (CIC), Taiwan, R.O.C. The authors would like to thank Dr. Y.-Z. Juang, CIC, and C.-C. Liu, Airwave Technology, Hsin-Chu, Taiwan, R.O.C., for their MMIC foundry coordination effort.

REFERENCES

[1] E. Alekseev and D. Pavlidis, "77 GHz high-isolation coplanar transmit–receive switch using InGaAs/InP PIN diodes," in *Gallium Arsenide Integrated Circuit Symp.*, 1998, pp. 177–180.

[2] S. G. Houng, T. Tsukii, and M. J. Schindler, "60–70 dB isolation 2–19 GHz MMIC switches," in *Gallium Arsenide Integrated Circuit Symp.*, 1989, pp. 173–176.

[3] N. Imai, A. Minakawa, and H. Okazaki, "Novel high isolation FET switches," *IEEE Trans. Microwave Theory Tech.*, vol. 44, pp. 685–691, May 1996.

[4] M. J. Schindler and A. Morris, "DC–40 GHz and 20–40 GHz MMIC SPDT switches," *IEEE Trans. Microwave Theory Tech.*, vol. MTT-35, pp. 1486–1493, Dec. 1987.

[5] P. Bermkopf, M. Schindler, and A. Bertrand, "A high power K/Ka-band monolithic T/R switch," in *IEEE Microwave and Millimeter-Wave Monolithic Circuits Symp. Dig.*, June 1991, pp. 15–18.

[6] G. L. Lan, D. L. Dunn, J. C. Chen, C. K. Pao, and D. C. Wang, "A high performance V-band monolithic FET transmit-receive switch," in *IEEE Microwave and Millimeter-wave Monolithic Circuits Symp. Dig.*, June 1988, pp. 99–101.

[7] M. Aust, H. Wang, R. Carandang, K. Tan, C. H. Chen, T. Trinh, R. Esfandiari, and H. C. Yen, "GaAs monolithic components development for Q-band phased array application," in *IEEE MTT-S Int. Microwave Symp. Dig.*, vol. 2, June 1992, pp. 703–706.

[8] M. Madihian, L. Desclos, K. Maruhashi, K. Onda, and M. Kuzuhara, "A sub-nanosecond resonant-type monolithic T/R switch for millimeter-wave systems applications," *IEEE Trans. Microwave Theory Tech.*, vol. 46, pp. 1016–1019, July 1998.
[9] D. L. Ingram, K. Cha, K. Hubbard, and R. Lai, "Q-band high isolation GaAs HEMT switches," in *Gallium Arsenide Integrated Circuit Symp.*, Orlando, FL, Nov. 1996, pp. 289–292.
[10] D. C. W. Lo, H. Wang, B. R. Allen, G. S. Dow, K. W. Chang, M. Biedenbender, R. Lai, S. Chen, and D. Yang, "Novel monolithic multifunctional balanced switching low-noise amplifiers," *IEEE Trans. Microwave Theory Tech.*, vol. 42, pp. 2629–2634, Dec. 1994.
[11] H. Mizutani, N. Funabashi, M. Kuzuhara, and Y. Takayama, "Compact DC–60-GHz HJFET MMIC switches using OHMIC electrode-sharing technology," *IEEE Trans. Microwave Theory Tech.*, vol. 46, pp. 1597–1603, Nov. 1998.
[12] K. Maruhashi, H. Mizutani, and K. Ohata, "Design and performance of a $K\alpha$-band monolithic phase shifter utilizing nonresonant FET switches," *IEEE Trans. Microwave Theory Tech.*, vol. 48, pp. 1313–1317, Aug. 2000.
[13] M. Hieda, K. Nakahara, K. Miyaguchi, H. Kurusu, Y. Iyama, T. Takagi, and S. Urasaki, "High-isolation series-shunt FET SPDT switch with a capacitor canceling FET parasitic inductance," *IEEE Trans. Microwave Theory Tech.*, vol. 49, pp. 2453–2458, Dec. 2001.
[14] *Sonnet User's Manual*, Sonnet Software Inc., Liverpool, NY.

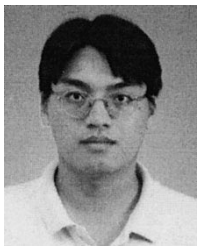

Kun-You Lin (S'98) was born in Taipei, Taiwan, R.O.C., in 1975. He received the B.S. degree in communication engineering from the National Chiao Tung University, Hsinchu, Taiwan, R.O.C., in 1998, and is currently working toward the Ph.D. degree in communication engineering at the National Taiwan University, Taipei, Taiwan, R.O.C.

His research interests include microwave and MMW circuit designs.

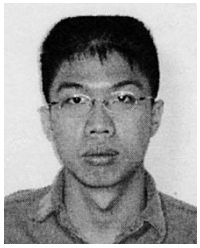

Yu-Jiu Wang was born in Taichung, Taiwan, R.O.C., in 1979. He received the B.S. degree in electrical engineering from the National Taiwan University, Taipei, Taiwan, R.O.C., in 2001.

He is currently with the R.O.C. Navy, and is scheduled to be discharged in June 2003. His current research interests are RF integrated-circuit design.

Dow-Chih Niu was born in Taipei, Taiwan, R.O.C., on August 28, 1956. He received the B. S. degree in electrophysics and M. S. degree in electronics engineering from the National Chiao Tung University, Hsinchu, Taiwan, R.O.C., in 1978 and 1982, respectively.

From 1982 to 1991, he was with the Chung-Shan Institute of Science and Technology (CSIST), Lung-Tang, Taiwan, R.O.C. From 1991 to 1993, he was with the University of California at Los Angeles. He is currently with CSIST, where he is in charge of the development of microwave and MMW circuits and subsystems.

Huei Wang (S'83–M'83–SM'95) was born in Tainan, Taiwan, R.O.C., on March 9, 1958. He received the B.S. degree in electrical engineering from the National Taiwan University, Taipei, Taiwan, R.O.C., in 1980, and the M.S. and Ph.D. degrees in electrical engineering from Michigan State University, East Lansing, in 1984 and 1987, respectively.

During his graduate study, he was engaged in research on theoretical and numerical analysis of EM radiation and scattering problems. He was also involved in the development of microwave remote detecting/sensing systems. In 1987, he joined the Electronic Systems and Technology Division, TRW Inc. He was a Member of the Technical Staff and Staff Engineer responsible for MMIC modeling of computer-aided design (CAD) tools, MMIC testing evaluation, and design. He then became the Senior Section Manager of the Millimeter Wave Sensor Product Section, RF Product Center, TRW Inc. In 1993, he visited the Institute of Electronics, National Chiao-Tung University, Hsin-Chu, Taiwan, R.O.C., and taught MMIC-related topics. In 1994, he returned to TRW Inc. In February 1998, he joined the faculty of the Department of Electrical Engineering, National Taiwan University, as a Professor.

Dr. Wang is a member of Phi Kappa Phi and Tau Beta Pi.